Power Electronics and Drives
3(38), No. 1, 2018 DOI: 10.2478/pead-2018-0002

sciendo

Power Electronics and Drives

Extended Kalman Filter Based Speed-Sensorless Load Torque and Inertia Estimations with Observability Analysis for Induction Motors

Research Article

Emrah Zerdali, Murat Barut

Niğde Ömer Halisdemir University, Faculty of Engineering, Electrical & Electronics Engineering Department Niğde, Turkey

Received August 21, 2017; Accepted February 16, 2018

Abstract: This paper aims to introduce a novel extended Kalman filter (EKF) based estimator including observability analysis to the literature associated with the high performance speed-sensorless control of induction motors (IMs). The proposed estimator simultaneously performs the estimations of stator stationary axis components of stator currents and rotor fluxes, rotor mechanical speed, load torque including the viscous friction term, and reciprocal of total inertia by using measured stator phase currents and voltages. The inertia estimation is done since it varies with the load coupled to the shaft and affects the performance of speed estimation especially when the rotor speed changes. In this context, the estimations of all mechanical state and parameters besides flux estimation required for high performance control methods are performed together. The performance of the proposed estimator is tested by simulation and real-time experiments under challenging variations in load torque and velocity references; and in both transient and steady states, the quite satisfactory estimation performance is achieved.

Keywords: *Extended Kalman filter • Induction motor • Load torque and inertia estimation • Speed-sensorless control • Observability analysis*

1. Introduction

Nowadays, there is a great deal of effort on speed-sensorless control of induction motors (IMs) due to the fact that IMs require low maintenance, can operate in harsh environmental conditions, and are easy to produce. The removal of the speed sensor has advantages such as cost reduction, enhanced drive safety, noise cancellation caused by sensor wiring, and so on. As a result of this intense interest, model based several methods have been proposed in the literature such as open-loop estimators (Bolognani et al., 2008), model reference adaptive systems (Kumar et al. 2015), observers (Atkinson et al., 1991; Lee and Blaabjerg, 2005; Zhao et al., 2014), etc. One of those methods, called extended Kalman filter (EKF), is a stochastic approach to nonlinear state and/or parameter estimation problem taking into account both the model errors and measurement noises.

In the literature, there are different studies in which EKF based state/parameter estimation is executed. Those studies can be divided into two groups: First group of studies (Alsofyani and Idris, 2016) in which the speed is assumed to be a constant state with the assumption that it changes slowly with respect to the electrical parameters and the second group of studies (Barut et al., 2007; Barut et al., 2012; Bogosyan et al., 2007; Inan and Barut, 2014; Zerdali and Barut, 2016; Zerdali and Barut, 2017) where the speed is included in the IM model with the help of equation of motion. The second group of studies is also needed to improve estimation performance especially in the low speed region, since it better reflects mechanical movements of IM by adopting IM as an electromechanical system; however, it is necessary to know the mechanical parameters such as unknown load torque, inertia varying with the load coupled to the shaft, and viscous friction (Barut et al., 2007).

* *Email: ezerdali@ohu.edu.tr, mbarut@ohu.edu.tr*

For this purpose, Barut et al. (2007) estimated the stator stationary axis components of rotor ($\varphi_{r\alpha}$ and $\varphi_{r\beta}$) or stator ($\varphi_{s\alpha}$ and $\varphi_{s\beta}$) fluxes together with the stator stationary axis components of stator currents ($i_{s\alpha}$ and $i_{s\beta}$), rotor mechanical speed (n_m), and load torque (t_L) including friction term. On the other hand, the estimation performance of Barut et al. (2007) is still influenced by the variations in electrical and mechanical parameters such as frequency and temperature based stator (R_s) and rotor (R_r) resistances, inertia (j_T), etc. In order to improve the estimation performance, Bogosyan et al. (2007) performed the estimations of $i_{s\alpha}$, $i_{s\beta}$, $\varphi_{r\alpha}$, $\varphi_{r\beta}$, n_m, t_L, R_s, and R_r using the braided EKF algorithm. Next, bi-input EKF (BI-EKF) algorithm, which uses two different IM model by periodically switching in a single EKF algorithm, is introduced to approximately reduce two times the required memory area instead of braided EKF utilizing consecutively switching two different EKF algorithms. Barut et al. (2012) estimated the similar parameters in Bogosyan et al. (2007) by using proposed BI-EKF. However, braided EKF in the study by Bogosyan et al. (2007) and BI-EKF in the study by Barut et al. (2012) estimate the R_s, and R_r at twice the sampling time ($2\times T$) while they estimate the $i_{s\alpha}$, $i_{s\beta}$, $\varphi_{r\alpha}$, $\varphi_{r\beta}$, n_m, and t_L at each sampling time (T), and they are still affected by the variations of j_T. Zerdali and Barut (2016) demonstrated the necessity of j_T estimation for speed/position sensorless speed/position control of IMs, and estimates the $i_{s\alpha}$, $i_{s\beta}$, $\varphi_{r\alpha}$, $\varphi_{r\beta}$, n_m, t_L, R_s, and $\gamma_T (1/j_T)$ by utilizing BI-EKF approach. Similarly to BI-EKF in the study by Barut et al. (2012), BI-EKF in the study by Zerdali and Barut (2016) estimated the R_s, R_r, t_L, and γ_T at twice the sampling time ($2\times T$) while it estimates the $i_{s\alpha}$, $i_{s\beta}$, $\varphi_{r\alpha}$, $\varphi_{r\beta}$, and n_m at each sampling time (T). In addition, Barut (2014) performed the estimations of the same parameters in the study by Zerdali and Barut (2016) except for γ_T, but it estimates mutual inductance instead of γ_T in order to improve estimation performance in the field weakening region. However, the design of BI-EKF algorithms in the study by Barut et al. (2012), Inan and Barut (2014) and Zerdali and Barut (2016), which use two different IM models by switching, are more complicated than standard EKF algorithms in the studies by Alsofyani and Idris (2016) and Barut et al. (2007).

The main contribution of this paper is to perform the simultaneously estimations of $i_{s\alpha}$, $i_{s\beta}$, $\varphi_{r\alpha}$, $\varphi_{r\beta}$, n_m, t_L including friction term, and γ_T for speed-sensorless control of IMs by utilizing the single EKF and assuming that measured phase currents and voltages are available. Namely, all mechanical state and parameters in addition to $i_{s\alpha}$, $i_{s\beta}$, $\varphi_{r\alpha}$, and $\varphi_{r\beta}$ are simultaneously estimated by using the standard EKF algorithm in which 7th order extended IM model is used. Thus, real-time velocity and flux estimations, which are not affected by changes in the load torque and inertia varying with load, have been achieved. Moreover, unlike Herman and Vaclavek (2012) performing the observability analysis for the continuous-time IM model, the observability analysis of the discrete-time IM model including the states of $i_{s\alpha}$, $i_{s\beta}$, $\varphi_{r\alpha}$, $\varphi_{r\beta}$, n_m, t_L, and γ_T is introduced to the literature in the scope of this paper.

This paper is organized into six sections. Section 1 introduces the literature related EKF based speed-sensorless control of IMs and the main contribution of this study. Sections 2 and 3 present the details of the 7th order extended IM model and the design of novel EKF based estimator, respectively. Section 4 shows the simulation performance of novel EKF based speed-sensorless drive system. Section 5 informs about the experimental setup used for the verification of the proposed EKF algorithm, and Section 6 demonstrates the real-time results confirming the effectiveness of novel EKF based estimator. Finally, Section 7 gives the conclusion.

2. Extended mathematical model of IM

In order to perform simultaneous estimations of t_L and $\gamma_T(1/j_T)$ together with $i_{s\alpha}$, $i_{s\beta}$, $\varphi_{r\alpha}$, $\varphi_{r\beta}$, and n_m by using measured phase currents and voltages, a rotor flux based 7th order extended IM model can be given in the following general form:

$$\mathbf{x}_e(k+1) = \mathbf{f}_e\left(\mathbf{x}_e(k), \mathbf{u}_e(k)\right) + \mathbf{w}_1(k) = \mathbf{A}_e\left(\mathbf{x}_e(k)\right)\mathbf{x}_e(k) + \mathbf{B}_e\mathbf{u}_e(k) + \mathbf{w}_1(k) \tag{1}$$

$$\mathbf{Z}(k) = \mathbf{h}_e\left(\mathbf{x}_e(k)\right) + \mathbf{w}_2(k) = \mathbf{H}_e\mathbf{x}_e(k) + \mathbf{w}_2(k) \tag{2}$$

where $\mathbf{x}_e$ is the extended state vector, $\mathbf{f}_e$ is the nonlinear function of the states and inputs, $\mathbf{A}_e$ is the system matrix, $\mathbf{B}_e$ is the input matrix, $\mathbf{u}_e$ is the control input vector, $\mathbf{h}_e$ is the function of the outputs, $\mathbf{H}_e$ is the measurement matrix, $\mathbf{w}_1$ and $\mathbf{w}_2$ are the process and measurement noises, respectively. The detailed state-space representations of IM model expressed in general form (1) and (2) can be given as follows:

$$\mathbf{x}_e(k) = \begin{bmatrix} i_{s\alpha}(k) & i_{s\beta}(k) & \varphi_{r\alpha}(k) & \varphi_{r\beta}(k) & \omega_m(k) & t_L(k) & \gamma_T(k) \end{bmatrix}^T$$

$$\mathbf{A}_e(\mathbf{x}_e(k)) =$$
$$\begin{bmatrix} 1-c_1 & 0 & c_2 & c_3\omega_m(k) & 0 & 0 & 0 \\ 0 & 1-c_1 & -c_3\omega_m(k) & c_2 & 0 & 0 & 0 \\ c_4 & 0 & 1-c_5 & -c_6\omega_m(k) & 0 & 0 & 0 \\ 0 & c_4 & c_6\omega_m(k) & 1-c_5 & 0 & 0 & 0 \\ -c_7\gamma_T(k)\varphi_{r\beta}(k) & c_7\gamma_T(k)\varphi_{r\beta}(k) & 0 & 0 & 1 & -T\gamma_T(k) & 0 \\ 0 & 0 & 0 & 0 & 0 & 1 & 0 \\ 0 & 0 & 0 & 0 & 0 & 0 & 1 \end{bmatrix}$$

$$\mathbf{B}_e = \begin{bmatrix} c_8 & 0 & 0 & 0 & 0 & 0 & 0 \\ 0 & c_8 & 0 & 0 & 0 & 0 & 0 \end{bmatrix}^T, \qquad \mathbf{u}_e(k) = \begin{bmatrix} v_{s\alpha} \\ v_{s\beta} \end{bmatrix},$$

$$\mathbf{H}_e = \begin{bmatrix} 1 & 0 & 0 & 0 & 0 & 0 & 0 \\ 0 & 1 & 0 & 0 & 0 & 0 & 0 \end{bmatrix}.$$

The coefficients are

$$c_1 = \left(\frac{R_S}{L_\sigma} + \frac{L_m^2}{L_\sigma L_r T_r}\right)T, \quad c_2 = \frac{L_m T}{L_\sigma L_r T_r}, \quad c_3 = \frac{L_m p_p T}{L_\sigma L_r}, \quad c_4 = \frac{L_m T}{T_r}, \quad c_5 = \frac{T}{T_r},$$

$$c_5 = p_p T,\ c_7 = \frac{3}{2}\frac{L_m}{L_r} p_p T,\ c_8 = \frac{T}{L_\sigma},$$

where R_s and L_s are the stator resistance and inductance, respectively. R_r and L_r are the rotor resistance and inductance referred to the stator side, respectively. L_m is the mutual inductance. T_r is the rotor time constant. $L_\sigma = \sigma L_s$ is the stator transient inductance; $\sigma = 1 - L_m^2/(L_s L_r)$ is the leakage or coupling factor. $v_{s\alpha}$ and $v_{s\beta}$ are stator stationary axis components of stator voltages. T is the sampling time.

$$\mathbf{O}_1 = \begin{bmatrix} \frac{\partial h_{e1}}{\partial x}(\boldsymbol{x}_k) \\ \frac{\partial h_{e2}}{\partial x}(\boldsymbol{x}_k) \\ \frac{\partial h_{e1}}{\partial x}(\boldsymbol{x}_{k+1})\frac{\partial f_e}{\partial x}(\boldsymbol{x}_k) \\ \frac{\partial h_{e2}}{\partial x}(\boldsymbol{x}_{k+1})\frac{\partial f_e}{\partial x}(\boldsymbol{x}_k) \\ \frac{\partial h_{e1}}{\partial x}(\boldsymbol{x}_{k+2})\frac{\partial f_e}{\partial x}(\boldsymbol{x}_{k+1})\frac{\partial f_e}{\partial x}(\boldsymbol{x}_k) \\ \frac{\partial h_{e2}}{\partial x}(\boldsymbol{x}_{k+2})\frac{\partial f_e}{\partial x}(\boldsymbol{x}_{k+1})\frac{\partial f_e}{\partial x}(\boldsymbol{x}_k) \\ \frac{\partial h_{e1}}{\partial x}(\boldsymbol{x}_{k+3})\frac{\partial f_e}{\partial x}(\boldsymbol{x}_{k+2})\frac{\partial f_e}{\partial x}(\boldsymbol{x}_{k+1})\frac{\partial f_e}{\partial x}(\boldsymbol{x}_k) \end{bmatrix} \tag{3}$$

$$\mathbf{O}_2 = \begin{bmatrix} \frac{\partial h_{e1}}{\partial x}(\boldsymbol{x}_k) \\ \frac{\partial h_{e2}}{\partial x}(\boldsymbol{x}_k) \\ \frac{\partial h_{e1}}{\partial x}(\boldsymbol{x}_{k+1})\frac{\partial f_e}{\partial x}(\boldsymbol{x}_k) \\ \frac{\partial h_{e2}}{\partial x}(\boldsymbol{x}_{k+1})\frac{\partial f_e}{\partial x}(\boldsymbol{x}_k) \\ \frac{\partial h_{e1}}{\partial x}(\boldsymbol{x}_{k+2})\frac{\partial f_e}{\partial x}(\boldsymbol{x}_{k+1})\frac{\partial f_e}{\partial x}(\boldsymbol{x}_k) \\ \frac{\partial h_{e2}}{\partial x}(\boldsymbol{x}_{k+2})\frac{\partial f_e}{\partial x}(\boldsymbol{x}_{k+1})\frac{\partial f_e}{\partial x}(\boldsymbol{x}_k) \\ \frac{\partial h_{e2}}{\partial x}(\boldsymbol{x}_{k+3})\frac{\partial f_e}{\partial x}(\boldsymbol{x}_{k+2})\frac{\partial f_e}{\partial x}(\boldsymbol{x}_{k+1})\frac{\partial f_e}{\partial x}(\boldsymbol{x}_k) \end{bmatrix} \tag{4}$$

As it is well-known, a model must be observable in order to use for state/parameter estimation; therefore, the observability analysis of IM model presented in (1) and (2) has to be done. For this aim, the rank condition in the studies by Alonge et al. (2015) and Vaclavek et al. (2013) is utilized and constitutes the sufficient condition for the IM model to be locally weakly observable. Using the approaches as in the studies by Alonge et al. (2015) and Vaclavek et al. (2013), the associated observability matrices are constructed as in (3) and (4):

In order to ensure the rank condition according to Alonge et al. (2015) and Vaclavek et al. (2013), at least one of $\mathbf{O}_1$ and $\mathbf{O}_2$ must be positive definite. Thus,

$$\det(\mathbf{O}_1) \neq 0 \vee \det(\mathbf{O}_2) \neq 0. \tag{5}$$

Assuming $x = x(k)$ and $x^+ = x(k+1)$, the corresponding determinants of $\mathbf{O}_1$ and $\mathbf{O}_2$ under the hypothesis of $x_3^+ - x_3 = 0$, $x_4^+ - x_4 = 0$, and $x_6^+ - x_6 = 0$ (constant rotor flux operation under no-load known as the worst case for speed-sensorless control of IM (Holtz, 2005; Zerdali and Barut, 2016)) are obtained as (6) and (7):

$$\det(\mathbf{O}_1) = -\chi |\phi_m|^4 \left(x_5 - x_5^+\right)\left(x_1 x_7^+ - x_7 x_1^+\right) \tag{6}$$

and

$$\det(\mathbf{O}_2) = -\chi |\phi_m|^4 \left(x_5 - x_5^+\right)\left(x_2 x_7^+ - x_7 x_2^+\right) \tag{7}$$

where $\chi = (3L_m^6 p_p^5 R_r T^7)/(2L_r^7 L_\sigma^5)$, $|\phi_m|$ is the amplitude of the maximum value of the flux components.

In order to ensure the rank condition under the constant rotor flux operation, Eqs. (6) and (7) must satisfy the condition in (8).

$$\phi_m \neq 0 \wedge x_5 \neq x_5^+ \wedge \left(x_1 x_7^+ \neq x_7 x_1^+ \vee x_2 x_7^+ \neq x_7 x_2^+\right) \tag{8}$$

As a result, IM model is observable if the condition in (8) is satisfied. The fluctuations in speed estimation stimulate the inertia estimation considering the equation of motion, however, this condition is no longer valid for dc condition due to constant zero speed ($x_5^+ = x_5 = 0$). Obtained observability results are compatible with existing studies in Alonge et al. (2015) and Herman and Vaclavek (2012). In addition, Herman and Vaclavek (2012) are emphasised that generated electrical moment must change with time to enable the simultaneously estimations of speed, load torque, and moment of inertia. Moreover, speed and load torque can be estimated in any case where the IM is observable.

3. Development of novel EKF algorithm

In order to develop the novel EKF based estimator, the conventional equations of the EKF algorithm using IM model in (1) and (2) can be given as follows:

$$\mathbf{F}_e = \left.\frac{\partial \mathbf{f}_e\left(\mathbf{x}_e(k), \mathbf{u}_e(k)\right)}{\partial \mathbf{x}_e(k)}\right|_{\hat{\mathbf{x}}_e(k)} \tag{9a}$$

$$\mathbf{N}(k) = \mathbf{F}_e(k)\mathbf{P}(k)\mathbf{F}_e(k)^T + \mathbf{Q} \tag{9b}$$

$$\mathbf{P}(k+1) = \mathbf{N}(k) - \mathbf{N}(k)\mathbf{H}_e^T\left(\mathbf{R} + \mathbf{H}_e\mathbf{N}(k)\mathbf{H}_e^T\right)^{-1}\mathbf{H}_e\mathbf{N}(k) \tag{9c}$$

$$\hat{\mathbf{x}}_e(k+1) = \mathbf{f}_e\left(\hat{\mathbf{x}}_e(k), \mathbf{u}_e(k)\right) + \mathbf{P}(k+1)\mathbf{H}_e^T\mathbf{R}^{-1}\left(\mathbf{Z}(k+1) - \mathbf{H}_e\hat{\mathbf{x}}_e(k)\right) \tag{9d}$$

where $\mathbf{F}_e$ is the function to linearize the nonlinear model. $\mathbf{P}$ and $\mathbf{N}$ are the covariance matrix of state estimation error and extrapolation error, respectively. $\mathbf{Q}$ is the covariance matrix of the system noise or known as modeling errors. $\mathbf{R}$ is the covariance matrix of the output noise or called as measurement noise or errors.

4. Simulation results

To verify the effectiveness of novel EKF algorithm, proposed estimation algorithm is included in a direct control vector (DVC) system as in Fig. 1. The rated parameters of the IM used in simulation are given in Table 1. The covariance matrices used in the novel EKF algorithm are carried out by trial-and-error method as

$\mathbf{Q}$=*diag*{10^{-8}, 10^{-8}, 10^{-8}, 10^{-4}, 10^{-3}, 10^{-2}},
$\mathbf{R}$=*diag*{10^{-10},10^{-10}},
$\mathbf{P}$=*diag*{10,10,10,10,10,10,10}.

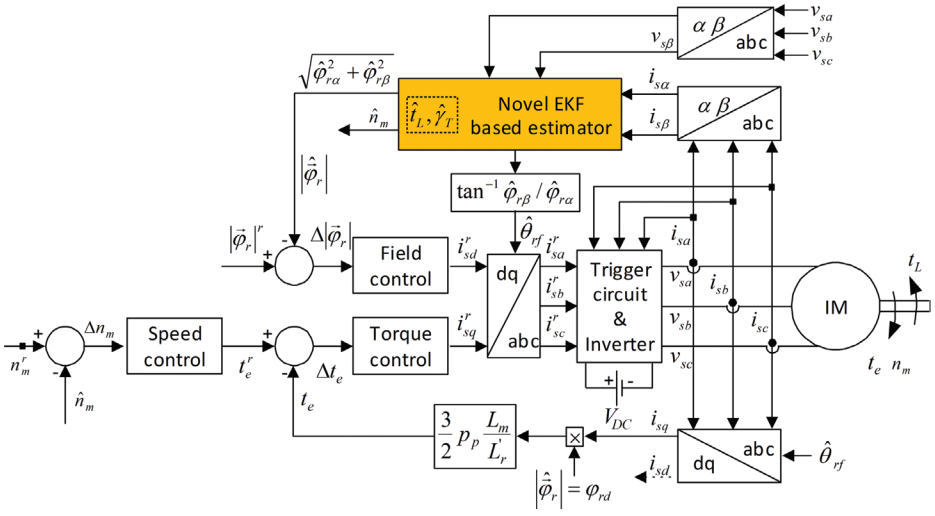

Fig. 1. The novel EKF based speed-sensorless direct vector control system.

In order to show the close-loop estimation performance of novel EKF based speed-sensorless DVC system, a scenario is determined as in Fig. 2 including several operating conditions. The resulting estimation and control performances of proposed speed-sensorless DVC system are presented in Fig. 3. In these figures, the "^" sign and $e_{(.)}$ mean the estimated state/parameter and the error defined as difference between measured and estimated ones, respectively.

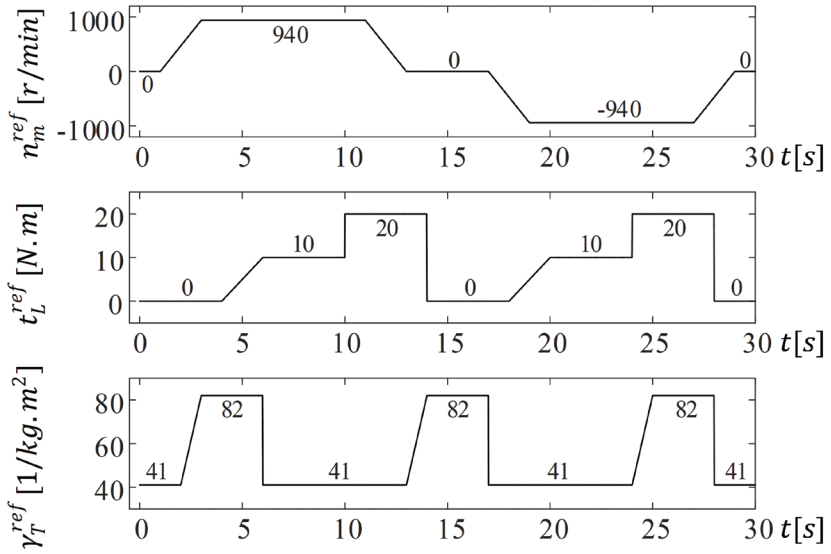

Fig. 2. Variations of n_m^{ref}, t_L^{ref} and γ_m^{ref} for the performance test of novel EKF

Table 1. Rated parameters of IM

P [kW]	V [V]	I [A]	n_m [rpm]	t_L [Nm]
2.2	380	5.9	940	22
R_s [Ω]	R_r [Ω]	L_{ls} [H]	L_{lr} [H]	L_m [H]
3.03	2.53	0.0116	0.0174	0.135

The following observations can be done considering the resulting estimation and control performances shown in Fig. 3:

- Despite zero-initial conditions of all estimated states and parameters, the estimations illustrated in Fig. 3 converge rapidly to their actual values; therefore the errors quickly fall to zero, too. In addition, it appears that the estimations are directly compatible to the observability results done in Section 2, e.g., γ_T estimation as in the time interval of $0 \le t \le 1$ s is not possible if constant electric torque is generated as described by Herman and Vaclavek (2012).
- The proposed speed-sensorless DVC system can overcome the variations in t_L and γ_T at high speeds for both forward and reverse rotations. Even at the transient states of the speed, it can tolerate the changes in t_L and γ_T.
- As seen in Fig. 3, the drive has capability to get over t_L and γ_T variations at zero speed region. Moreover, it can operate at zero rotor flux frequency for a satisfactory time interval (refer to $0 \le t \le 1$ s, $13 \le t \le 17$ s, and $29 \le t \le 30$ s in Fig. 3).

5. Experimental setup

In order to demonstrate the performance of novel EKF algorithm, the experimental test setup illustrated in Fig. 4 is utilized. A 3-phase squirrel cage type IM having the specifications given in Table 1 is loaded by a 30 Nm Foucault brake. The 5000 lines/rev encoder is used for confirming the speed estimation while the 50 Nm torque transducer is employed to verify the load torque estimation. For measuring the phase currents and voltages, LA55-P/SP1 and LV100-400 are utilized, respectively. The IM is also driven by an AC drive in order to test the EKF algorithm with space vector pulse-with modulated voltages and thus currents in the stator stationary frame. A power PC-based DS1104 controller, which is compatible with Matlab Simulink software and includes 64-bit floating-point processor with 250 MHz clock, is used to develop the novel EKF. Thus, the novel EKF algorithm developed with the utilization of Matlab Simulink C/C++ S–function is used for real-time experiments.

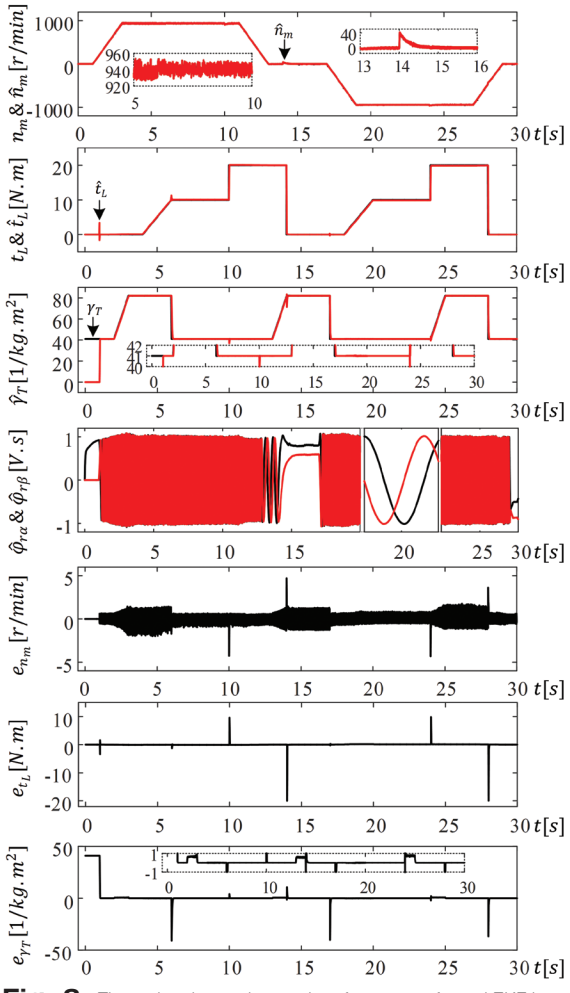

Fig. 3. The estimation and control performance of novel EKF based DVC system under closed-loop.

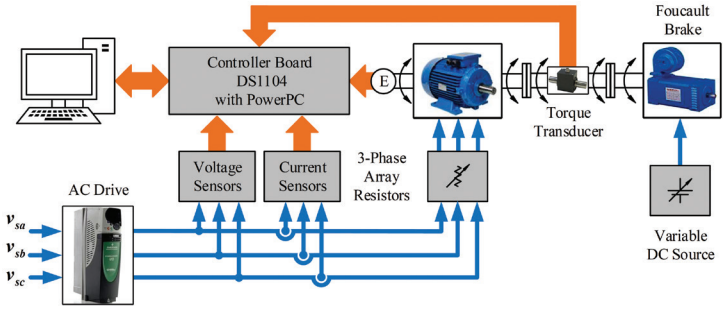

Fig. 4. The block diagram of open-loop experimental setup used for verifying novel EKF algorithm.

6. Experimental results

In order to illustrate the effectiveness of the novel EKF algorithm, challenging scenarios are set up as in Figs. 5–9. In these scenarios,

- the proposed algorithm is fed by the voltages and currents obtained from the ac drive shown in Fig. 4, and thus the real-time performance of the proposed algorithm is tested in open-loop case. In other words, the AC drive

is only used for supplying the IM and the proposed EKF based estimator and there is no-feedback to the AC drive from the estimator.

- the estimation performance of the proposed novel EKF is tested by starting with zero initial conditions in Fig. 5, under step-type load torque variations in Fig. 6, under speed reversals with or without load in Fig. 7, at both low and zero speeds in Fig. 8, and at speeds from zero speed to rated speed in Fig. 9.
- the Foucault brake cannot apply high load torque to the IM at very low speeds due to its the torque–speed characteristics. For example, no-eddy currents are induced in the Foucault brake's disk at zero-speed, and therefore, no-torque is generated (Barut et al., 2012).

The "^" sign and $e_{(.)}$ mean the estimated state/parameter and the error defined as difference between measured and estimated ones, respectively. During the experiments, all initial conditions of states and parameters are set to zero and sampling time T is taken as 75 μs. Also, the tuning of EKF is still open to research (Zerdali and Barut, 2017) even though there are some approaches as in the study by Bittanti and Savaresi (2000) in the literature. It is known that

- increasing diagonal elements of **Q** causes faster tracking response together with the increased noises on the estimated states/parameters,
- **P** is effective at the initial convergences of the estimations,
- **R** can be calculated as in the study by Barut et al. (2012) or assumed the matrix to be tuned as in the study by Bittanti and Savaresi (2000).

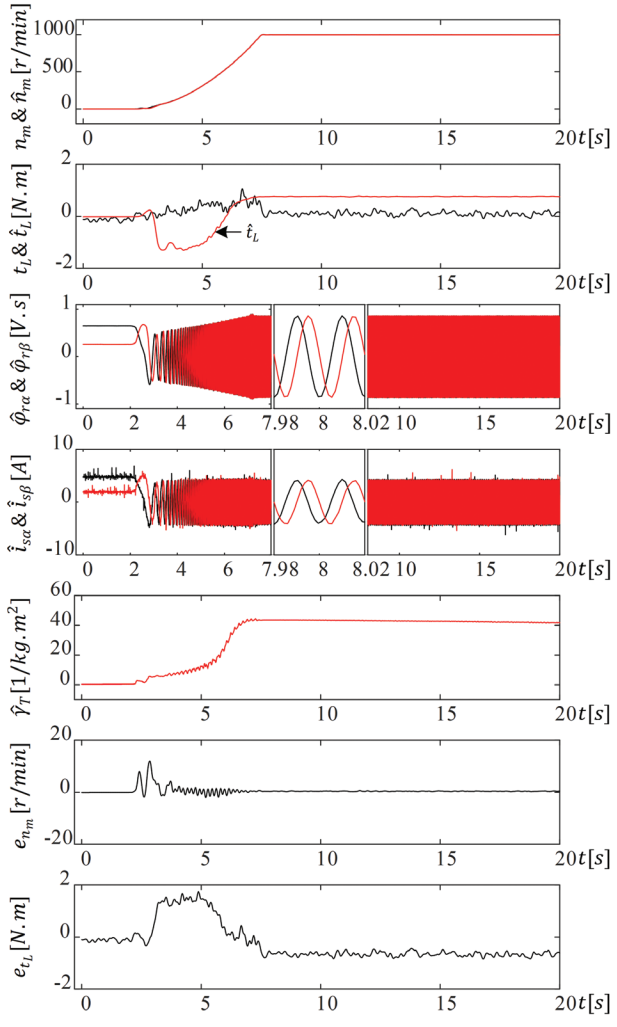

Fig. 5. The estimation results of novel EKF starting with zero initial conditions.

In this paper, the values of **P**, **Q**, and **R** are tuned by trial-and-error method until satisfactory estimation performance is obtained as follows:

$\mathbf{Q}=diag\{10^{-1}, 10^{-1}, 10^{-7}, 10^{-7}, 10^{-4}, 10^{-5}, 10^{-8}\}$,
$\mathbf{R}=diag\{10^{-1}, 10^{-1}\}$,
$\mathbf{P}=diag\{10, 10, 10, 10, 10, 10, 10\}$

The details of the scenarios and the observations related to the estimation results are listed below:

- In the first scenario given in Fig. 5, the acceralation is achieved by manually changing the input frequency of the AC drive. The aim of this scenario is to show the initial estimation performance of novel EKF algorithm; therefore, IM is initialized while initial conditions of all states and parameters are zero. Since the changes in the inertia are effective during the transient state, the transient state is kept longer to clearly demonstrate how well

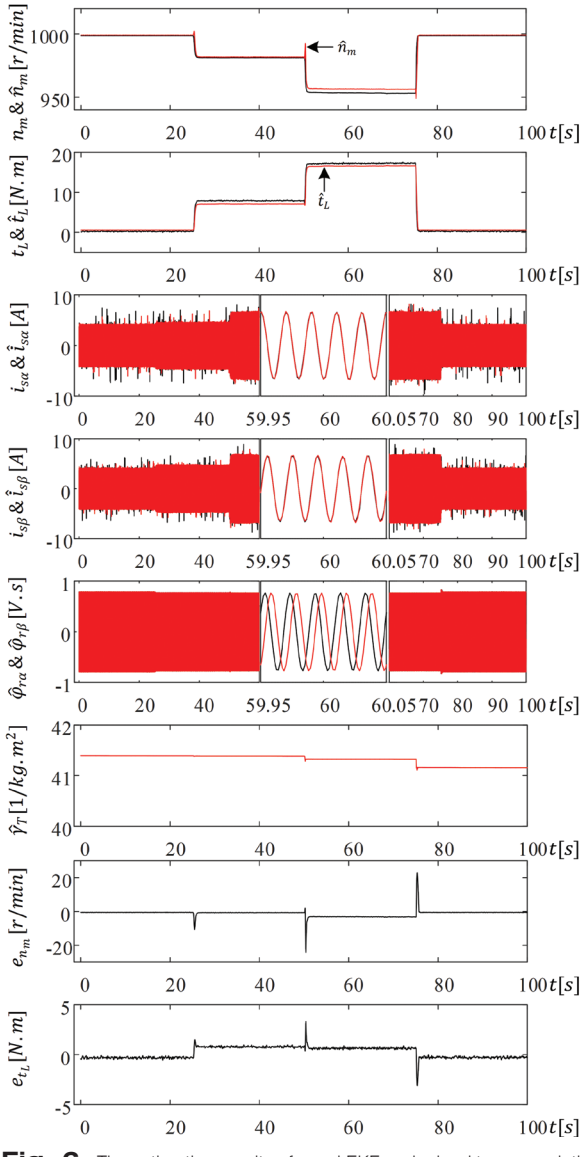

Fig. 6. The estimation results of novel EKF under load torque variations.

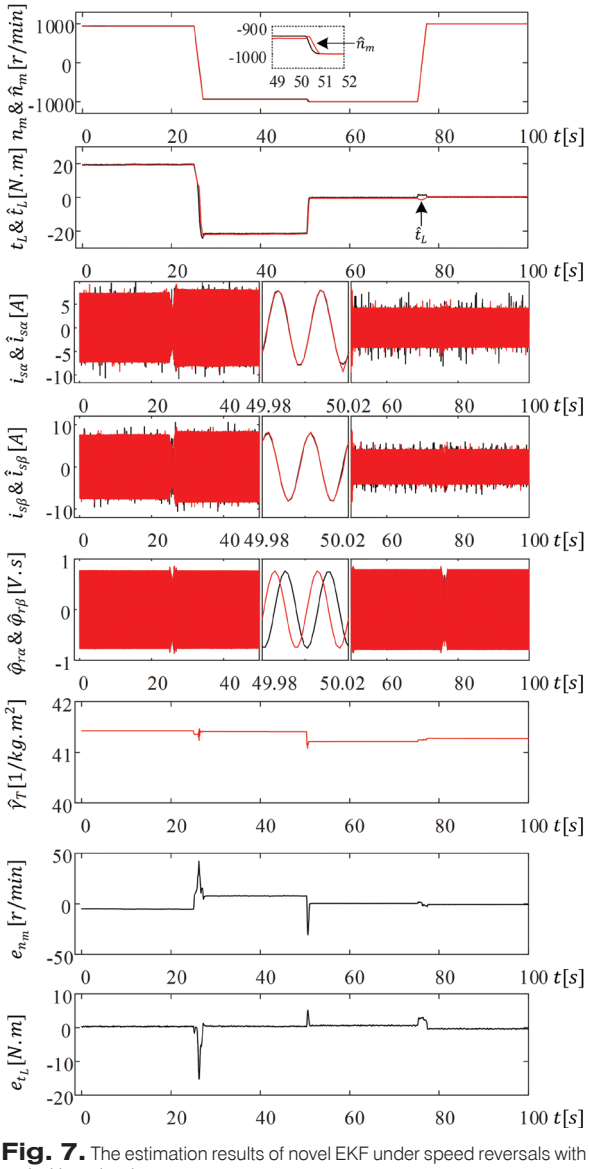

Fig. 7. The estimation results of novel EKF under speed reversals with and without load torque.

γ_T-estimation is obtained. As seen in Fig. 5, all of them converge the actual values immediately. The errors in transient states quickly converge to zero in steady states. Also it is observed that the proposed algorithm has also satisfactory estimation performances for a shorter transient states than one in Fig. 5.

- The second scenario shown in Fig. 6 focuses on the estimation performance of novel EKF under step-type load torque variations at rated speed. For this aim, IM is loaded to 8 Nm and 18 Nm at t = 25 s and t = 50 s, respectively. It successfully overcomes these step-type variations. Increasing load torque causes the acceptable steady state errors in ω_m and t_L estimations. Also, in the figures the speed has been given in r/min instead of rad/s in order to show the errors clearly. The small variations in γ_T at the transient states mean a slight or negligible variations in j_T.
- The third scenario presented in Fig. 7 purposes to demonstrate the estimation performance under speed reversals with or without load. In this scenario, IM is loaded to 20 Nm in the time interval of $0 \le t \le 50$ s, and its speed is reversed at t =25 s. Next, load is removed at approximately t =50 s, and its speed is reversed again at t =75 s. Thus, the speed of IM is reversed at both loaded and unloaded conditions. In Fig. 7, it seems that the estimation errors have a slight increase in the loaded conditions as in Fig. 6. Considering the estimation performance in Fig. 7, novel EKF can handle the speed reversals both in loaded and unloaded conditions.

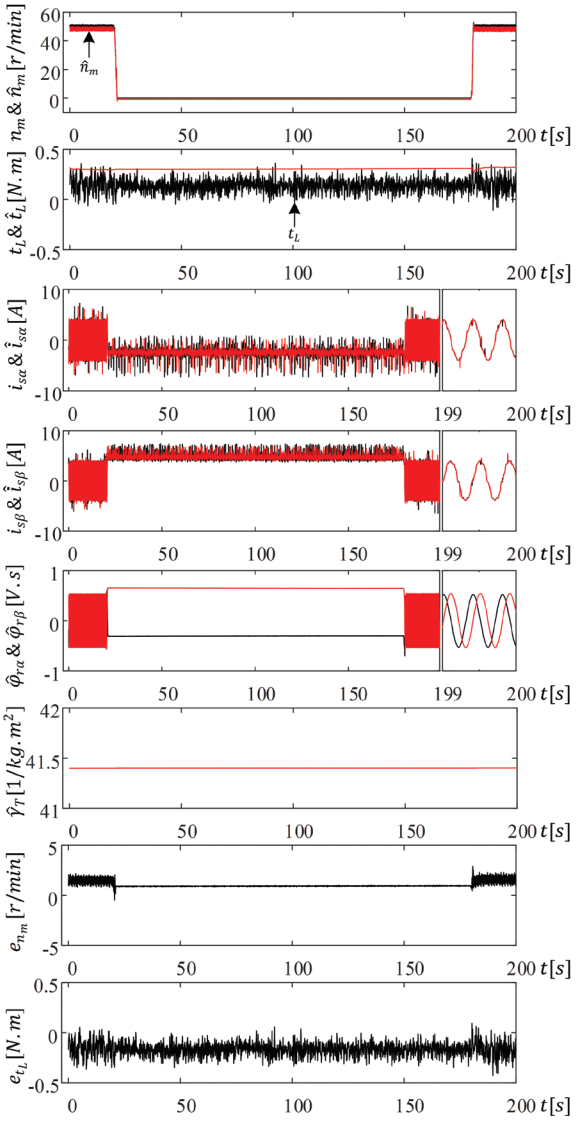

Fig. 8. The estimation results of novel EKF both at rated and zero speeds with or without load torque.

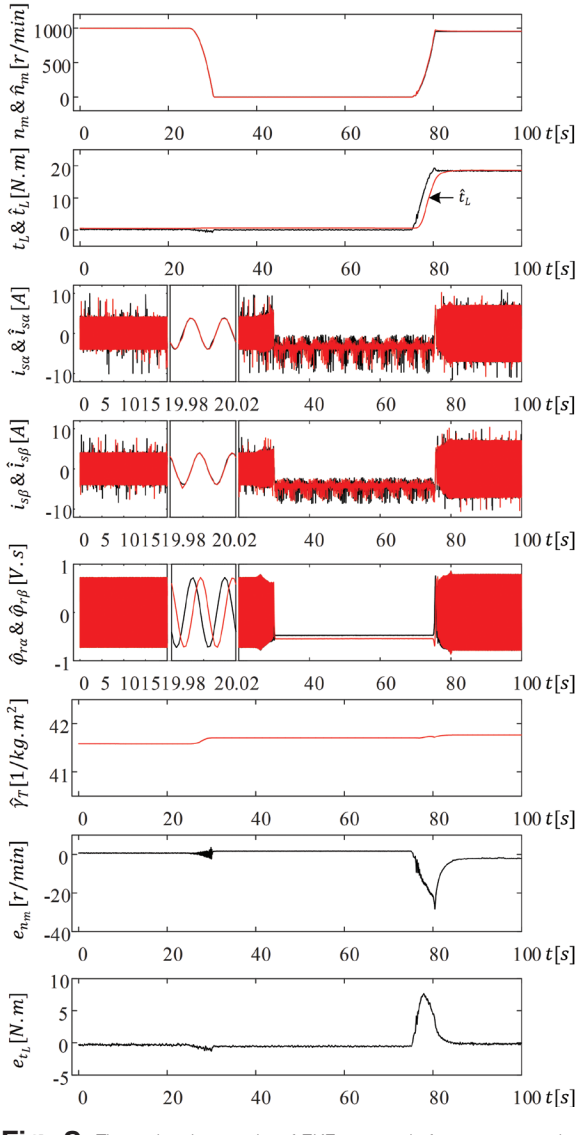

Fig. 9. The estimation results of EKF at speeds from zero speed to nominal speed.

- The fourth scenario aims to verify the effectiveness of novel EKF algorithm in low and zero speed regions. In this scenario, the speed is decreased to zero at t =20 s when IM runs at 50 r/min. Next, IM speeds up to 50 r/min at t =180 s again while IM continues to run at zero speed in the time interval of 20 ≤ t ≤ 180 s. According to the results obtained for the fourth scenario, the proposed method can operate in the zero rotor flux frequency where most of model-based methods in the literature fail because no-induction occurs from the stator to the rotor side. It has been also proven that the model-based estimation is impossible only when constant rotor magnetic flux condition (dc condition) is fulfilled (Alonge et al., 2015; Herman and Vaclavek, 2012). This case occurs at zero speed operation under no-load. Although IM model is unobservable at dc condition, the performed estimations does not diverge from the actual values for a long time, and then the proposed algorithm can detect the changes in states and parameters since the EKF naturally takes the system noise into account, which helps to improve the estimation performance at zero stator frequency.
- The fifth scenario seen in Fig. 9 is the most challenging scenario because most of model-based estimation techniques in the literature are fail at zero rotor flux frequency and cannot operate at both high and zero speeds at the same time. In this scenario, the speed is reduced to zero as it runs the nominal speed without load, and IM continues to operate at zero speed for about 50 seconds. Next, the IM speeds up to rated speed with 19 Nm load. Resulting estimation performance proves that the novel EKF can overcome this challenging scenario despite the zero speed reference.
- The last scenario in Fig. 10 is performed to show the superiority of the proposed 7th order EKF method over the 6th order EKF algorithm estimating $i_{s\alpha}$, $i_{s\beta}$, $\varphi_{r\alpha}$, $\varphi_{r\beta}$, n_m, and t_L except for j_T as the study by Barut et al. (2007). As seen in Fig. 10, the variations of 0.5×j_{TN}, 2×j_{TN} and 3×j_{TN} occurring in j_T causes estimation errors in the transient states, this scenario calls for the estimation of j_T (or $\gamma_T = 1/j_T$).

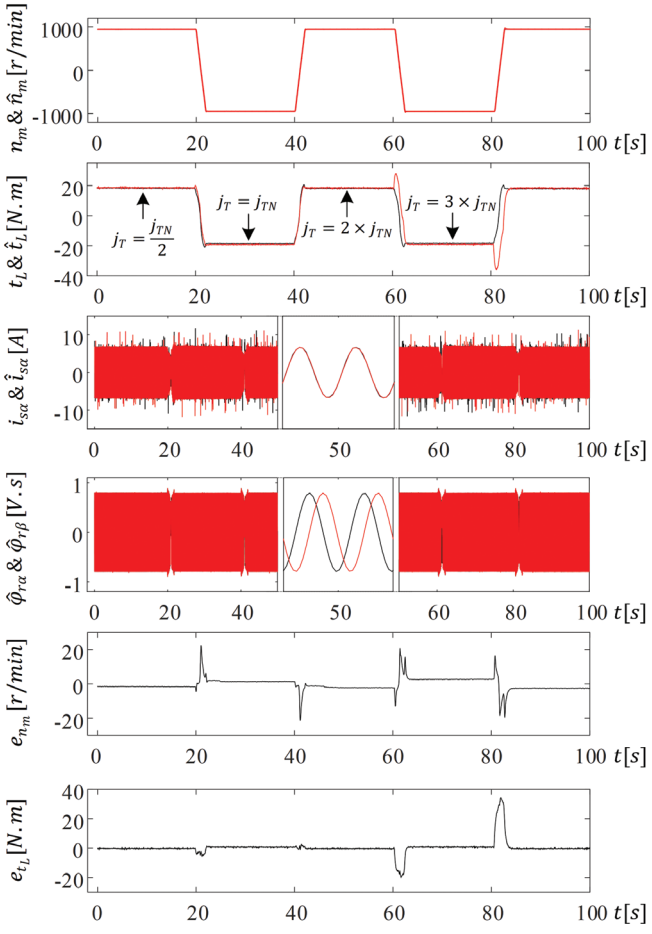

Fig. 10. The estimation results of sixth-order EKF algorithm estimating $i_{s\alpha}$, $i_{s\beta}$, $\varphi_{r\alpha}$, $\varphi_{r\beta}$, n_m, and t_L except for j_T

7. Conclusion

In this paper, a novel EKF based estimator with observability analysis, which fulfills the simultaneous estimations of i_{sa}, $i_{s\beta}$, φ_{ra}, $\varphi_{r\beta}$, n_m, t_L including friction term, and γ_T by using the measured phase currents and voltages, is firstly introduced for high performance speed-sensorless control of IMs. In order to demonstrate the effective performance of the proposed estimation technique, it is tested by real-time experiments under challenging variations of load torque and velocity references. Considering the obtained real-time results, the quite satisfactory estimation performance has been achieved in both transient and steady states, and the proposed method can operate between zero speed and nominal speed regions in which most of methods in the literature fail. In addition, the inertia, which changes with load coupled to the shaft and affects the speed estimation performance, is also estimated; Thus, proposed estimation technique is robust to the inertia variations. In this context, all the mechanical parameters and state in addition to the flux estimation required for high performance control methods are estimated. However, the proposed algorithm is still sensitive the R_S, R_r, and L_m variations which deteriorate the estimation performance; Therefore, it requires the changing R_S, R_r, and L_m (in field weakening region) knowledge.

References

Alonge, F., Cangemi, T., D'Ippolito, F., Fagiolini, A. and Sferlazza, A. (2015). Convergence Analysis of Extended Kalman Filter for Sensorless Control of Induction Motor. *IEEE Transactions on Industrial Electronics*, 62(4), pp. 2341-2352.

Alsofyani, I. M. and Idris, N. R. N. (2016). Lookup-Table-Based DTC of Induction Machines with Improved Flux Regulation and Extended Kalman Filter State Estimator at Low-Speed Operation. *IEEE Transactions on Industrial Informatics*, 12(4), pp. 1412-1425.

Atkinson, D., Acarnley, P. and Finch, J. (1991). Observers for Induction Motor State and Parameter Estimation. *IEEE Transactions on Industry Applications*, 27(6), pp. 1119-1127.

Barut, M., Bogosyan, S. and Gokasan, M. (2007). Speed-Sensorless Estimation for Induction Motors Using Extended Kalman Filters. *IEEE Transactions on Industrial Electronics*, 54(1), pp. 272-280.

Barut, M., Demir, R., Zerdali, E. and Inan, R. (2012). Real-Time Implementation of Bi Input-Extended Kalman Filter-Based Estimator for Speed-Sensorless Control of Induction Motors. *IEEE Transactions on Industrial Electronics*, 59(11), pp. 4197-4206.

Bittanti, S. and Savaresi, S.M. (2000). On the Parameterization and Design of an Extended Kalman Filter Frequency Tracker. *IEEE Transactions on Automatic Control*, 45(9), pp. 1718-1724.

Bogosyan, S., Barut, M. and Gokasan, M. (2007). Braided Extended Kalman Filters for Sensorless Estimation in Induction Motors at High-Low/Zero Speed. *IET Control Theory Applications*, 1(4), pp. 987-998.

Bolognani, S., Peretti, L. and Zigliotto, M. (2008). Parameter Sensitivity Analysis of an Improved Open-Loop Speed Estimate for Induction Motor Drives. *IEEE Transactions on Power Electronics*, 23(4), pp. 2127-2135.

Herman, I. and Vaclavek, P. (2012). Load torque and moment of inertia observability analysis for alternating current drive sensorless control. In: *38th Annual Conference on IEEE Industrial Electronics Society IECON 2012,* Montreal, Canada, pp. 1864-1869.

Holtz, J. (2005). Sensorless Control of Induction Machines - With or Without Signal Injection? *IEEE Transactions on Industrial Electronics*, 53(1), pp. 7-30.

Inan, R. and Barut, M. (2014). Bi Input-Extended Kalman Filter-Based Speed-Sensorless Control of an Induction Machine Capable of Working in the Field-Weakening Region. *Turkish Journal of Electrical Engineering and Computer Science*, 223, pp. 588-604.

Kumar, R., Das, S., Syam, P. and Chattopadhyay, A. (2015). Review on Model Reference Adaptive System for Sensorless Vector Control of Induction Motor Drives. *IET Electric Power Applications*, 9(7), pp. 496-511.

Lee, K.-B. and Blaabjerg, F. (2005). Reduced-Order Extended Luenberger Observer Based Sensorless Vector Control Driven by Matrix Converter with Nonlinearity Compensation. *IEEE Transactions on Industrial Electronics*, 53(1), pp. 66-75.

Vaclavek, P., Blaha, P. and Herman, I. (2013). AC Drive Observability Analysis. *IEEE Transactions on Industrial Electronics*, 60(8), pp. 3047-3059.

Zerdali, E. and Barut, M. (2016). Novel Version of Bi Input-Extended Kalman Filter for Speed-Sensorless Control of Induction Motors with

Estimations of Rotor and Stator Resistances, Load Torque, and Inertia. *Turkish Journal of Electrical Engineering & Computer Sciences*, 24(5), pp. 4525-4544.

Zerdali, E. and Barut, M. (2017). The Comparisons of Optimized Extended Kalman Filters for Speed-Sensorless Control of Induction Motors. *IEEE Transactions on Industrial Electronics*, 64(6), pp. 4340-4351.

Zhao, L., Huang, J., Liu, H., Li, B. and Kong, W. (2014). Second-Order Sliding Mode Observer with Online Parameter Identification for Sensorless Induction Motor Drives. *IEEE Transactions on Industrial Electronics*, 61(10), pp. 5280-5289.